Simultaneously boost diffusion length and stability of perovskite for high performance solar cells

Chao Liang,[1,a] Dandan Zhao,[1,a] Pengwei Li,[3,a] Bo Wu,[7] Hao Gu,[1] Jiacheng Zhang,[4] Teck Wee Goh,[2] Shi Chen,[1] Yonghua Chen,[6] Zhendong Sha,[4] Guosheng Shao,[5] Tze Chien Sum*[2] and Guichuan Xing*[,1]*

[1]Joint Key Laboratory of the Ministry of Education, Institute of Applied Physics and Materials Engineering, University of Macau, Avenida da Universidade, Taipa, Macau 999078, P. R. China.

[2]Division of Physics and Applied Physics, School of Physical and Mathematical Sciences, Nanyang Technological University, 21 Nanyang Link, Singapore 637371, Singapore.

[3]Key Laboratory of Green Printing, Institute of Chemistry, Chinese Academy of Sciences (ICCAS), Beijing Engineering Research Center of Nanomaterials for Green Printing Technology, Beijing National Laboratory for Molecular Sciences (BNLMS), Beijing 100190, P. R. China.

[4]State Key Laboratory for Strength and Vibration of Mechanical Structures, School of Aerospace Engineering, Xi'an Jiaotong University, Xi'an 710049, P. R. China.

[5]State Centre for International Cooperation on Designer Low-Carbon and Environmental Material (SCICDLCEM), School of Materials Science and Engineering, Zhengzhou University, Zhengzhou 450001, P. R. China.

[6]Key Laboratory of Flexible Electronics (KLOFE) & Institution of Advanced Materials (IAM), Jiangsu National Synergetic Innovation Centre for Advanced Materials (SICAM), Nanjing Tech University (NanjingTech), Nanjing 211816, Jiangsu, P. R. China.

[7]Institute of Electronic Paper Displays, South China Academy of Advanced Optoelectronics, South China Normal University, Guangzhou, Guangdong Province, 510006, P. R. China.

Corresponding Author

*E-mail: zhendongsha@mail.xjtu.edu.cn (Z. Sha), Tzechien@ntu.edu.sg (T. C. Sum) and gcxing@umac.mo (G. Xing)

[a] C. Liang, D. Zhao and P. Li contributed equally to this work.

Keywords: perovskite solar cells; diffusion length; high performance; stability

Abstract

Organic-inorganic hybrid metal-halide perovskites, such as methylammonium lead iodide, have emerged as amazing semiconductors with immense potential in thin film photovoltaic owing to their impressive diffusion lengths. However, the instability of these perovskites in ambient air, due to the presence of hydrophilic and volatile organic cation, hinders their further commercialization. Although low-dimensional perovskite solar cells (PSCs) show better stability than conventional three-dimensional (3D) devices, the low power conversion efficiency (PCE) is delivered, due to the decline of carrier mobility and diffusion length. Here, a large organic cation, tert-butylammonium (t-BA), is incorporated into the 3D perovskite, which not only enhances the crystal stability, but also greatly reduces the trap density and improves the mobility of the perovskite film, leading to ~1.8 μm electron and hole diffusion lengths. High-performance PSCs based on t-$BA_{0.1}[Cs_{0.05}(FA_{0.83}MA_{0.17})_{0.95}]_{0.9}Pb(I_{0.83}Br_{0.17})_3$ with champion PCEs of 20.62% (19.8% ± 0.4%) for 0.04 cm^2 and 14.54% for 20.8 cm^2 are demonstrated. More importantly, with humidity of 45-55%, the solar cells could sustain 80% of their "post burn-in" PCE after continuous working under light (AM1.5G, 100 mW cm^{-2}) in air for 1174 h. This lifetime is 63% longer than that (718 h) of the control $Cs_{0.05}(FA_{0.83}MA_{0.17})_{0.95}Pb(I_{0.83}Br_{0.17})_3$ PSCs.

Graphical Abstract

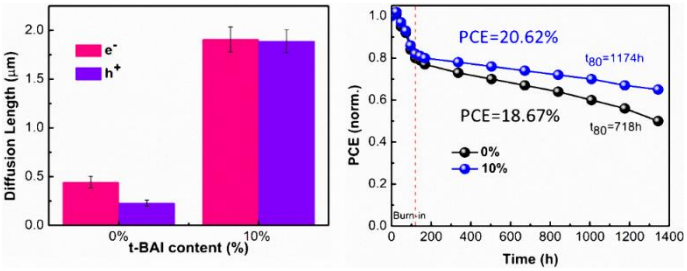

A large organic cation, tert-butylammonium, is incorporated into the 3D perovskite, leading to ~1.8 μm electron and hole diffusion lengths. The efficiency of 20.62% for 0.04 cm^2 and 14.54% for 20.8 cm^2 are demonstrated. More importantly, the solar cells could sustain 80% of their "post burn-in" PCE after continuous working under light (AM1.5G, 100 mW cm^{-2}) in air for 1174 h.

Research highlights

1. First report presenting concrete evidences (experimental and modelling) on that the large size t-BA could be doped in 3D perovskite crystal lattice.

2. First report on the clear photophysical picture of the charge carrier dynamics and transports in the t-BA doped 3D perovskites.

3. Based on the t-BA doped perovskite, the power conversion efficiency and stability of solar cells are boosted simultaneously.

1. Introduction

Organic-inorganic lead halide perovskites ($APbX_3$, A is organic cation, X is halide anion) have recently emerged as one of the most promising photovoltaic semiconductor materials, because of their extraordinary photoelectrical desired features, including excellent ambipolar charge mobilities [1-3], small exciton binding energies [4–5], long charge carrier diffusion lengths [6], low defect densities [7-8], desirable band gap, high absorption coefficient [9-10], and low-cost solution processability [11-12]. The power conversion efficiency (PCE) of small-laboratory-based perovskite solar cells (PSCs) has reached the certified 23.3%, approaching the efficiency of the mainstream solar cells based on crystallized silicon [13]. However, the long-term stability issue of perovskite active layers in the ambient air, due to presence of hydrophilic and volatile methylammonium cation, hinders their commercialization [14].

Composition engineering or doping is one of the most effective ways to tailor semiconductor physical properties. In three-dimensional (3D) lead-halide perovskites, by replacing the single-cation with multiple-cations of suitable ionic radius (R), such as $CH_3NH_3^+$ (methylammonium, MA), $CH_3(NH2)_2^+$ (formamidinium, FA), or Cs^+, both the stability and optoelectronic performance can be greatly improved. Here, all the cations used must fit into the inorganic Pb-I framework while maintaining a cubic crystal structure with Goldschmidt tolerance factor ($t = (R_A + R_I)/\sqrt{2}(R_{Pb} + R_I)$) between 0.8 and 1. With these multiple-cation perovskites, the solar cell functional time could be improved from dozens of hours to few hundreds hours [15-17]. However, stability improvements are still far from satisfactory for commercialization, which typically needs more than ten years' service lifetime.

In order to further improve the stability, the perovskite crystal lattice could be terminated by incorporating some large radius organic cations ($t > 1$). Then the dimensionality is reduced from 3D to quasi-2D, 1D or even 0D. The large organic cation layers could function as moisture and oxygen passivation layers and ion migration blocking layers. The stability is largely enhanced with

these low dimensional perovskites. Unfortunately, this method typically sacrifices the charge transport for the insulating spacer cations. The PCEs of the devices based on these low dimensional perovskites are lower than that with the 3D counterparts, because of the shorter charge carrier diffusion length, lower charge mobility and wider band gap [18-25]. Therefore, the challenge remains to develop high-performance PSCs, which would exhibit the long-term stability while still possessing high PCE.

More recently, researchers found that the 3D $MAPbI_3$ could be doped with slightly large guanidinium cation ($t = 1.03$), which could remarkably improve the stability without sacrificing the PCE [26]. This method may provide pathways to effectively solve the perovskite stability issue for commercialization. However, this guanidinium cation is the solely reported candidate with suitable large size that could be doped inside the 3D perovskite crystal. Here, a new large branched alkylammonium organic cation, tert-butylammonium (t-BA), is introduced into the $Cs_{0.05}(FA_{0.83}MA_{0.17})_{0.95}Pb(I_{0.83}Br_{0.17})_3$ triple-cation system. Surprisingly, this incorporation does not reduce the perovskite dimensionality but retains the original 3D frame, which is essential for effective photo-generated carrier extraction in devices. The density functional theory (DFT) calculations suggest that the t-BA doping can greatly increase the 3D perovskite crystal formation energy, therefore, increase the stability. The large cation may compensate at the expense of the neighboring cavities where the small cation localizes, preserving its stable 3D structure [26]. Electrical and optoelectronic characterizations revealed that the t-BA markedly reduces the trap density, increases the charge carrier mobility and diffusion lengths in this new perovskite structures. Therefore, high-performance PSCs based on t-$BA_{0.1}[Cs_{0.05}(FA_{0.83}MA_{0.17})_{0.95}]_{0.9}Pb(I_{0.83}Br_{0.17})_3$ with a champion PCE of 20.62% (19.8% ± 0.4%) for 0.04 cm^2 and 14.54% for 20.8 cm^2 are demonstrated. More importantly, the solar cells sustain

80% of their "post burn-in" PCE after 1174 h, which is much longer than the control device (718 h), under continuous light illumination (AM1.5G, 100 mW cm^{-2}) in an ambient environment at 45-50 ^{o}C and with 45-55% humidity.

2. Results and discussion

To illustrate the difference between the dopant and traditional cations, the molecular structures of the t-BA and typical cation MA are shown in Fig. 1a. The ionic radius of t-BA is ~ 292 pm ($t \sim 1.06$), which is near 25% larger than that of MA. Based on size consideration, only low-dimensional perovskite will be formed when t-BA is mixed with PbI_2. In this work, in order to achieve better performance and higher stability than conventional $MAPbI_3$, the $Cs_{0.05}(FA_{0.83}MA_{0.17})_{0.95}Pb(I_{0.83}Br_{0.17})_3$ triple-cation system was utilized as the control sample (see Methods for details) [27]. Then the large branched t-BA with different molar ratios was incorporated into this triple-cation system. The X-ray diffraction (XRD) patterns of the deposited $t\text{-}BA_x[Cs_{0.05}(FA_{0.83}MA_{0.17})_{0.95}]_{1-x}Pb(I_{0.83}Br_{0.17})_3$ perovskite films with X = 0%, 5%, 10%, 15%, 20%, 30%, 50% and 100% are shown in Fig. 1b and c. The results clearly show that the deposited films feature the typical 3D perovskite peaks when X is less than 20%, which indicates these films could maintain the 3D perovskite crystal structure with suitable amount t-BA incorporation. Magnification of the XRD peaks at (110) and (220) on variation of the t-BA content is illustrated in Fig. 1c. The diffraction peaks shift towards low 2θ values with increasing t-BA concentration, because the ionic diameter of t-BA is larger than that of other cations (Cs, FA, MA). These results indicate that the incorporated t-BA cations should enter the 3D perovskite crystal lattice. However, when the t-BA doping concentration (X) is further increased to over 20%, new XRD peaks located at 10.4° and 10.9° appear. These new peaks suggest the formation of other perovskite phases other than the 3D perovskite [26]. To further confirm the t-BA doping in 3D perovskite crystal lattice,

the surface chemical composition and chemical environment of the pristine and doped (X = 10%) films were examined with X-ray photoelectron spectroscopy (XPS). Both films show a relative Pb/(I+Br) ratio of ~ 3.0, which is consistent with the theoretical stoichiometry in 3D perovskite structures (Fig. S1). However, the results also show that the N 1s peak intensity in MA/t-BA is significantly enhanced in the doped film, which indicates that the incorporation of t-BA does change the composition of the perovskite cations.

The linear absorption spectra of the pristine and t-BA doped mixed perovskite films are presented in Fig. 1d. The results show that the absorption edges of the t-BA doped films (about 770 nm) are very close to that of the pristine $Cs_{0.05}(FA_{0.83}MA_{0.17})_{0.95}Pb(I_{0.83}Br_{0.17})_3$ film, ensuring efficient light harvesting by the doped perovskite. A slight blue shift is observed with increased t-BA content, indicative of a widening of the bandgap. In addition, the t-BA incorporation also yields a mild steady-state photoluminescence (PL) peak blue shift from 780 nm to 760 nm (Fig. S2). The blue shift of absorption and PL spectra should be caused by the large t-BA doping induced lattice distortion. To further understand electronic contribution of the t-BA incorporation, femtosecond transient absorption (TA) spectroscopy was performed on the pristine (X = 0%) and doped (X = 10%) perovskite films. In TA measurements (Fig. S3), the perovskite films were excited with a femtosecond laser pulse (425 nm), the photo-induced changes in absorption spectrum are then probed with a time-delayed laser-generated white light probe pulse. The typical two photo bleaching (PB) bands peaked around 470 nm and 750 nm of the 3D perovskite are observed for both the pristine and doped films [6], which indicates compositions of the two films should be dominated by 3D perovskite. No other excitonic absorption bleaching peaks associated with low dimensional perovskites could be clearly resolved for X = 10% film, which further

suggests that the low dimensional perovskites formed with low content t-BA incorporation are negligible.

To understand the effect of t-BA incorporation on the morphology of perovskite films, we performed scanning electron microscopy (SEM) on the perovskite surface with different t-BA content (Fig. 1e-l). The results clearly show that with suitable amount t-BA doping (X ≤ 10%), the grain size of the perovskite film could be enlarged. The minor doping may reduce the activation energy for crystallization [28]. Therefore, with the increased doping concentration of t-BA, the crystallization of perovskite can be accelerated, leading to an enlarged grain size. However, if the doping concentration is further increased to over 10%, the grain size decreases and the cracks and pinholes appear, which should be induced by that the t-BA exists as an impurity between the grains and inhibits the grains growth. Ultimately, the film prepared with 10% t-BA shows the largest grain size and the best film quality, which will be beneficial to the device performance. Notably, the 2D and quasi-2D layered perovskite structure is not observed in all proportions of t-BA (X ≤ 50%), indicating that this method maintains the original 3D crystal structure, consistent with our above results of XPS and TA spectroscopy.

To investigate the electronic properties and the structural stability, DFT calculations were performed via the CASTEP code [29-30]. Here, in order to simplify the calculation, we used t-$BA_xMA_{1-x}PbI_3$ instead of the complex t-$BA_x[Cs_{0.05}(FA_{0.83}MA_{0.17})_{0.95}]_{1-x}Pb(I_{0.83}Br_{0.17})_3$ structure, and selected a few representative doping values (X = 0, 0.125, 0.25) (Note S1 and Fig. S4). To evaluate the stabilities of the proposed mixed t-$BA_xMA_{1-x}PbI_3$ structures, their formation enthalpies, ΔH_f, are estimated via

$$(x)\ \text{t-BAI} + (1-x)\ \text{MAI} + PbI_2 \rightarrow \text{t-}BA_xMA_{1-x}PbI_3 \quad (1)$$

A greater value of enthalpy in the exothermic reaction implies a greater system stability. [25] The calculated formation enthalpy for $MAPbI_3$ is a positive value of 0.097 eV, which is similar to that reported in a recent DFT-GGA calculation (ΔH_f = 0.060 eV) [31]. This indicates that the $MAPbI_3$ is intrinsically unstable, which is consistent with previous experimental results demonstrating a positive formation enthalpy for $MAPbI_3$ of 0.359 eV [32]. For t-$BA_{0.125}MA_{0.875}PbI_3$ and t-$BA_{0.25}MA_{0.75}PbI_3$, the calculated ΔH_f are -0.015 eV and 0.301 eV, respectively. Compared with pure $MAPbI_3$ perovskite, t-$BA_{0.25}MA_{0.75}PbI_3$ has a larger positive enthalpy of formation, while t-$BA_{0.125}MA_{0.875}PbI_3$ has a negative one. Such a trend has an important implication that the substitution of t-BA for 12.5% MA in the $MAPbI_3$ structure results in a significant increase of the system stability. However, the system stability is weakened when the substitution of t-BA for MA is further increased to 25%.

To demonstrate the application of t-BA doped perovskite in light harvesting, the planar heterojunction solar cells with t-$BA_x[Cs_{0.05}(FA_{0.83}MA_{0.17})_{0.95}]_{1-x}Pb(I_{0.83}Br_{0.17})_3$ used as the light absorption layer were constructed. Fig. 2a shows a typical cross-section SEM image of the devices, consisting of fluorine-doped tin-oxide (FTO)/TiO_2 (40 nm)/ t-$BA_x[Cs_{0.05}(FA_{0.83}MA_{0.17})_{0.95}]_{1-x}Pb(I_{0.83}Br_{0.17})_3$ (400 nm)/spiro-OMeTAD (250 nm)/Au (80 nm) [33]. The current–voltage (J–V) response of the devices, obtained with a scan rate of 100 mV s^{-1} and back scan from open-circuit to short-circuit condition, is shown in Fig. 2b. The results clearly show that the open circuit voltage (V_{OC}) increases with increasing t-BA doping concentration, which may correlate with the slightly increasing band gap. To further explain the promotion of V_{OC}, ultraviolet photoelectron spectroscopy (UPS) measurements on the pristine (X = 0%) and doped (X = 10%) perovskite films were performed. The results show a change in work function from 4.22 to 4.26 eV between the pristine and the doped film, leading to a further 160 meV Fermi level (E_F) shift towards the valence

band maximum (E_V) (Fig. S5 and 6). Such E_F shift indicates a more p-type nature of the doped perovskite, which is the right direction to achieve increased Voc in a cell [34]. In addition, the optimal short circuit current (J_{SC}) and fill factor (FF) can be obtained with 10% t-BA doping, which is in good agreement with the best crystal quality and most improved charge carrier diffusion length. Eventually, the optimum device based on t-$BA_{0.1}[Cs_{0.05}(FA_{0.83}MA_{0.17})_{0.95}]_{0.9}Pb(I_{0.83}Br_{0.17})_3$ shows outstanding performance with J_{SC} of 23.68 mA cm^{-2}, V_{OC} of 1.20 V, FF of 72.57% and PCE of 20.62%, which is higher than the champion PSC based on $Cs_{0.05}(FA_{0.83}MA_{0.17})_{0.95}Pb(I_{0.83}Br_{0.17})_3$ (J_{SC} of 22.93 mA cm^{-2}, V_{OC} of 1.16V, FF of 70.21% and PCE of 18.67%). The detailed photovoltaic parameters of the PSCs employing X = 0% or X = 10% from forward bias to short circuit (FB-SC) and from short circuit to forward bias (SC-FB) are shown in Table S1. Notably, negligible photocurrent hysteresis is observed for the PSCs with 10% t-BA by changing the scanning directions, as shown in Fig. 2c. This negligible hysteresis could be attributed to the reduced trap state density and increased carrier mobility [35-36], which will be illustrated in the following sections. Fig. 2d shows the incident photon-to-electron conversion efficiencies (IPCEs) for the PSCs based on X = 0% and X = 10% device. Compared to the X = 0% device (integrated current 20.55 mA cm^{-2}), X = 10% device (integrated current 22.25 mA cm^{-2}) shows larger IPCE values in the whole visible range from 300 to 780 nm, which is consistent with the larger J_{SC} observed. In Fig. 2e-h, based on 20 cells per condition, the statistical results (J_{SC}, V_{OC}, FF and PCE) are presented for the t-BA doping concentration dependent device performance. The detailed photovoltaic parameters are shown in Table 1. The results clearly show the average PCE could be improved from 17.4 ± 0.8% to 19.8 ± 0.4% by replacing the pristine perovskite with the t-BA doped (10%) perovskite as the light harvesting layer. The PCE is enhanced, rather than reduced by incorporation suitable amount of large size t-BA into the perovskite layer.

To explore the photophysical mechanisms for the device performance improvement with large t-BA doping, we performed photoluminescence (PL) and time-resolved PL (TRPL) measurements on the pristine and doped (10%) perovskite films. Fig. 3a shows the PL kinetics of the two films, from which we can extract a carrier lifetime of 40 ± 1 ns for the pristine and 380 ± 10 ns for the doped films, respectively. The one order of magnitude increased PL lifetime indicates the significant reduction of non-radiative recombination centres with t-BA incorporation. This result is consistent with the above theoretical prediction that the substitution of a small amount of original cation with lager t-BA leads to an improved 3D lattice stability, and therefore the formation of a hybrid system with less defects. The charge carrier diffusion properties of the two films were also examined with PL quenching method. After depositing a layer of electron or hole extraction material, the corresponding carrier diffusion and extraction can result in a drop of the intrinsic PL intensity and acceleration of PL decay rate. This is clearly seen from the TRPL of both perovskite films (~ 400 nm thick) with spiro-OMeTAD (for hole extraction) and PCBM (for electron extraction) layers (Fig. S7). The PL lifetimes drastically drop to 10.4 ± 0.1 ns and 22.9 ± 0.1 ns for the pristine film with PCBM and spiro-OMeTAD, respectively. For the 10% t-BA doped film, the more efficient charge transfer leads to more pronounced lifetime drop to 6.9 ± 0.3 ns and 7.0 ± 0.1 ns in the presence of PCBM and spiro-OMeTAD layers, respectively.

With the drift-diffusion model developed previously, the corresponding carrier mobilities and diffusion lengths were extracted [6]. The obtained electron and hole mobilities for the pristine film are 1.9 ± 0.4 $cm^2s^{-1}V^{-1}$ and 0.5 ± 0.1 $cm^2s^{-1}V^{-1}$, respectively. The corresponding values for the 10% t-BA doped film are improved to 3.7 ± 0.4 $cm^2s^{-1}V^{-1}$ and 3.6 ± 0.4 $cm^2s^{-1}V^{-1}$, respectively (Fig. 3b). This improvement should be mainly attributed to less carrier-defect scattering, enlarged crystal

size and no dimensionality reduction. Together with the lifetimes, the carrier diffusion lengths could be calculated according to the following equation:

$$L = \sqrt{\mu k_B T / e\tau} \quad (2)$$

where μ is the carrier mobility, k_B is the Boltzmann constant, T is the temperature, e is the elementary charge and τ is the carrier lifetime. The diffusion lengths of the pristine perovskite film are calculated to be 440 ± 60 nm and 230 ± 30 nm for the electrons and holes, respectively. The corresponding lengths are boosted to 1910 ± 130 nm and 1890 ± 120 nm for the optimal t-BA doped perovskite film (Fig. 3c). We should note, the above μm and balanced electron/hole diffusion lengths are among the best reported values for 3D perovskite polycrystalline films [6,37] and much longer than that of the low-dimensional perovskites [38]. These superior carrier diffusion lengths are originated from the improved 3D perovskite stability with t-BA doping.

Lastly, a previous theoretical model developed by us to estimate the trap density with photo-injected carrier density dependent integrated PL intensity was also employed to compare these two films [39]. Briefly speaking, at low photo-injected carrier density, the carriers mainly fill the low-lying traps and undergo non-radiative recombination. Whilst at high injection regime after the traps are filled, the carriers undergo mainly radiative recombination, leading to prominent PL. The PL intensity versus photo-injected carrier density for the two films are shown in Fig. 3d and the fitted curves with the model are also presented with the solid lines. From the fitting, the trap density for the pristine film is extracted to be 2.4×10^{16} cm^{-3}, which is drastically reduced to 3.1×10^{15} cm^{-3} for the 10% t-BA doped film. The results are also in good agreement with those values obtained from electrical method (Note S2 and Fig. S8), consolidating the reduction of defects with the t-BA cation.

We conducted a steady-state output test for 150 s at maximum power point (MPP) tracking. The steady-state output profiles (Fig. 4a) show PCE of 17.18% and 19.45% under 1 Sun AM1.5G illumination measured in air, for X = 0% and X = 10% devices. In addition, the X = 10% device shows a faster light response than the X = 0% one, which is consistent with the lower trap density and higher carrier mobility in the t-BA doped perovskite. The long-term stability of the X = 0% and X = 10% PSCs were examined under continuous light illumination (AM1.5G, 100 mW cm^{-2}) in an ambient environment at 45-50 ^{o}C with 45-55% humidity [40]. The results are shown in Fig. 4b. To carry out a quantitative analysis, we fit the post 'burn-in' section of the PCE to a straight line and extrapolate the curve back to zero time to obtain the PCE at t = 0 [41]. The lifetime, 80% degradation (t_{80}) post "burn-in" PCE, for the X = 10% device is 1174 h, which is 63% longer than that of the X = 0% device (718 h). The detailed photovoltaic parameters are shown in Fig. S9. According to previous reports, the degradation of the perovskite films is likely to proceed via active defects [42]. Hence, we attribute the enhanced stability to the optimized crystal structure and reduced crystal defects. Based on the X = 10% perovskite active layer, large area (6×6 cm^2) modules were fabricated (as shown in Fig. 4c). The champion device consisting of 11 series connection cells with an active area of 20.8 cm^2 shows a high PCE of 14.54% (Fig. 4d), which is higher than the control one with pristine perovskite (12.64%) (Fig. S10). The detailed statistical photovoltaic parameters from 5 cells per condition are shown in Table S2. In addition, this X = 10% module maintains 92% of its original PCE after 1000 h, in ambient air with 45-55% humidity (Fig. S11). By contrast, the PCE of 0% device drops very fast, around 82% of their initial efficiency lost after 1000 h. These results indicate incorporation of t-BA could achieve high efficiency and improve stability even in an up-scaled device. Thus, our work opens up a new approach to fabricate large-area, high-performance, and high-stability PSCs.

3. Conclusions

In summary, with a suitable amount of large size t-BA doping into the 3D perovskite crystal lattice, the carrier diffusion lengths and crystal stability could be simultaneously improved. Optical and electrical studies revealed that the t-BA incorporation (10%) could effectively reduce trap density, hence increasing the charge carrier mobilities and diffusion lengths. Both experimental characterization and theoretical calculation confirm that moderate t-BA doping can stabilize the 3D perovskite crystal structure. Therefore, the planar PSCs based on optimal t-BA doped perovskite show a champion PCE of 20.62% (19.8% ± 0.4%), which is higher than 18.67% (17.4 ± 0.8%) of the control one without doping. Furthermore, a large size (6 × 6 cm^2) high PCE (14.54%) solar module was constructed with this t-BA doped perovskite, which demonstrates the potential for upscaling. More importantly, the doped solar cells sustain 80% of their "post burn-in" PCE after 1174 h, which is much longer than the control one (718 h) did. Our results show the large size t-BA doping could greatly increase the metal-halide perovskite stability without sacrificing the high photovoltaic performance. This method paves the way to effectively solve the perovskite stability issue for commercialization.

4. Experimental Section

Materials: FAI (99.5%), MABr (99.5%) and spiro-MeOTAD (99.8%) were purchased from Xi'an Polymer Light Technology Corp. $TiCl_4$ (99.9%), CsI (99.99%), PbI_2 (99.99%), $PbBr_2$ (99.99%) and all anhydrous solvents (DMF, DMSO, acetonitrile, chlorobenzene, ethyl alcohol, acetone, isopropyl alcohol) were purchased from Alfa–Aesar. All chemicals were used without further purification.

Fabrication of perovskite films: The $Cs_{0.05}(FA_{0.83}MA_{0.17})_{0.95}Pb(I_{0.83}Br_{0.17})_3$ perovskite films were deposited from a precursor solution containing FAI (183.09 mg), PbI_2 (513.9 mg), MABr (24.42

mg) and $PbBr_2$ (86.33 mg) in anhydrous DMF (0.8 ml) and DMSO (0.2 ml). Then CsI (45 µl), predissolved as a 1.5 M stock solution in DMSO, was added to the mixed perovskite precursor to achieve the desired triple cation composition. The t-$BA_x[Cs_{0.05}(FA_{0.83}MA_{0.17})_{0.95}]_{1-x}Pb(I_{0.83}Br_{0.17})_3$ precursor solution was achieved according to the corresponding proportion. The obtained solution was stirred at 65 ºC for 12 h in a nitrogen-filled glovebox. Then the solution was spin coated in a two-step successive procedure at 1500 and 6000 rpm for 15 and 25 s respectively. During the second step, 150 µL of chlorobenzene was dripped on the spinning substrate 10 s prior to the end of the procedure. The perovskite-precursor film was then annealed at 110 ºC for 60 min on a hotplate.

Fabrication of PSCs: F-doped SnO_2 (FTO) with a sheet resistance of 8 Ω sq^{-1} and an optical transmission of greater than 83% in the visible range were used. After thoroughly washing with de-ionized water, acetone, ethanol, and isopropanol, the clean FTO glasses were treated under UV-ozone for 15 min. Yellow polyimide tape was kept to the back side and to the two edges on the front side for contacting, in order to ensure that there is no deposition of TiO_2 at the back side and at the edges. The solution of $TiCl_4$ (stored in the freezer) was diluted to 200 mM at 0 ºC. The FTO with the tapes were then put into this solution and kept in an oven at 70 ºC for 1 h in a closed beaker. After 1 h, the FTO were washed with ethanol and water and dried at 100 ºC in air for 1 h. The perovskite light harvesting layer was deposited using aforementioned method. The hole transport material, 2,2,7,7-tetrakis(N,N-di-pmethoxyphenylamine)-9,9-spirobifluorene (spiro-MeOTAD), was then deposited by spin coating at 3000 r.p.m. for 30 s. The spin-coating formulation was prepared by dissolving 72.3 mg spiro-MeOTAD, 28.8 mL 4-tert-butylpyridine (t-BP), and 17.5 mL of a stock solution of 520 mg mL^{-1} lithium bis(trifluoromethylsulphonyl)imide

(LiTFSI) in acetonitrile in 1mL chlorobenzene. Finally, an Au electrode was deposited by thermal evaporation through a shadow mask at a base pressure of 10^{-7} Torr.

Characterization: The phase structure information was characterized on a Rigaku (RINT-2500) X-ray diffractometer (Cu Ka radiation, λ=1.5418 Å). SEM images were obtained via a field emission scanning electron microscope (JEM-7500F). UV–vis–NIR fluorescence spectrophotometer absorption spectra were recorded on a Shimadzu UV 3600 spectrophotometer at room temperature. PL (excitation at 532 nm) was measured with Edinburgh Instruments (FLSP920). XPS were detected on Multilab 2000 XPS system, using a monochromatic Mg Kα source and a charge neutralizer. All the binding energies were referenced to the C 1s peak of the surface adventitious carbon at 284.6 eV. The UPS measurements were performed on a PHI5000 Versa Probe instrument. The UPS radiation was generated by a He-gas discharge lamp (He Iα at 21.22 eV). The J-V curves characteristics were recorded with a Keithley 2400 source meter and 425 W collimated Xenon lamp (Newport) calibrated with the light intensity to 100 mW cm^{-2} under AM 1.5 G solar light condition by the certified silicon solar cell. The J-V curves were obtained by reverse (forward bias (1.3 V) → short circuit (0 V)) or forward (short circuit (0 V) → forward bias (1.3 V)) scan with different scan rate. Incident photon-to-electron conversion efficiency (IPCE) was obtained on a computer-controlled IPCE system (Newport).

Transient absorption: The wide band femtosecond TA spectra of the perovskite films were taken using the Ultrafast System HELIOS TA spectrometer. The laser source was the Coherent Legend regenerative amplifier (150 fs, 1 KHz, 800 nm) seeded by a Coherent Vitesse oscillator (100 fs, 80 MHz). The broadband probe pulses (420–780 nm) were generated by focusing a small portion (around 10 mJ) of the fundamental 800 nm laser pulses into a 2 mm sapphire plate. 425-nm pump pulses were generated from a Light Conversion TOPAS-C optical parametric amplifier.

Transient photoluminescence: Time resolved PL was collected using an Optronis Optoscope™ streak camera system which has an ultimate temporal resolution of ~10 ps. The pump source was 500 nm laser pulses with pulse width ~ 50 fs that was generated from an optical parametric amplifier (OperASolo) coupled to a one-box integrated Ti-Sapphire amplifier (Libra, Coherent).

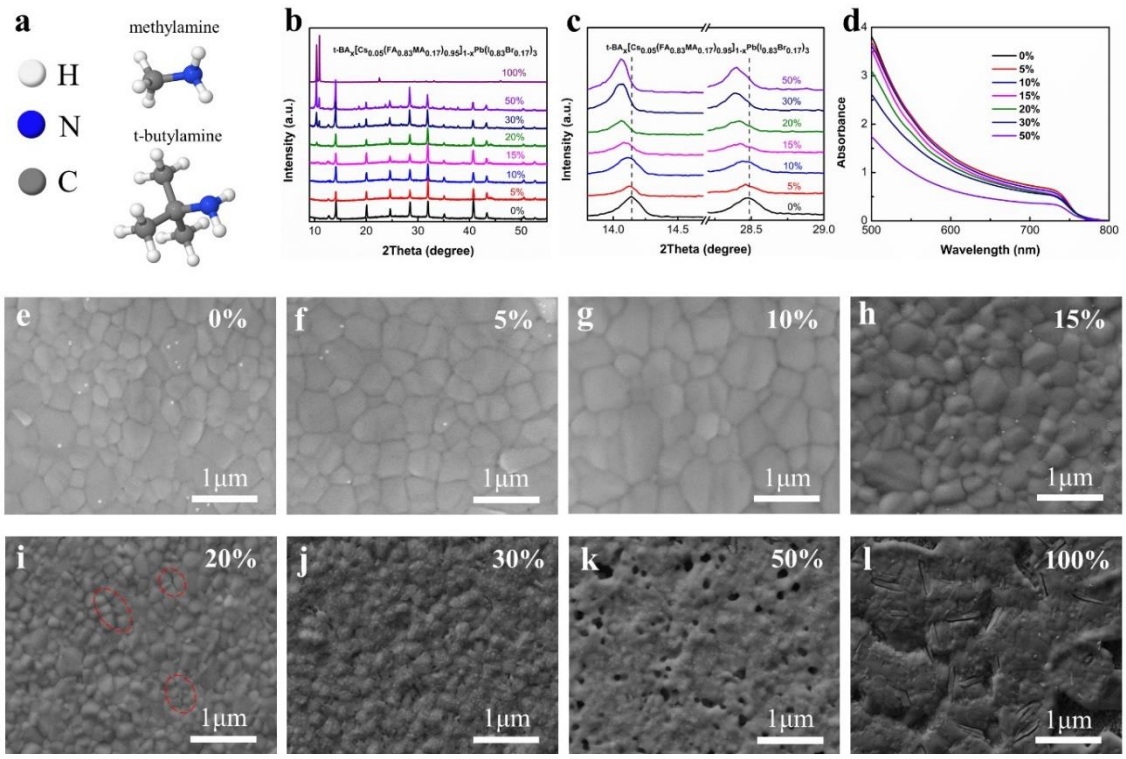

Fig. 1. Basic characteristics of t-$BA_x[Cs_{0.05}(FA_{0.83}MA_{0.17})_{0.95}]_{1-x}Pb(I_{0.83}Br_{0.17})_3$ perovskite films. (a) The molecular structures of the methylamine and tert-butylammonium. (b) X-Ray diffraction (XRD) pattern for the mixed perovskite films containing different percentages of t-BA. (c) Magnification of the XRD peaks at (110) and (220) on variation of the t-BA content. (d) Absorption spectra of the mixed perovskite films containing $X \leq 50\%$. (e-l) Top-view scanning electron microscopy (SEM) images of the mixed perovskite films derived from different percentages of t-BA deposited on TiO_2 films at X = 0%, 5%, 10%, 15%, 20%, 30%, 50%, 100%, respectively.

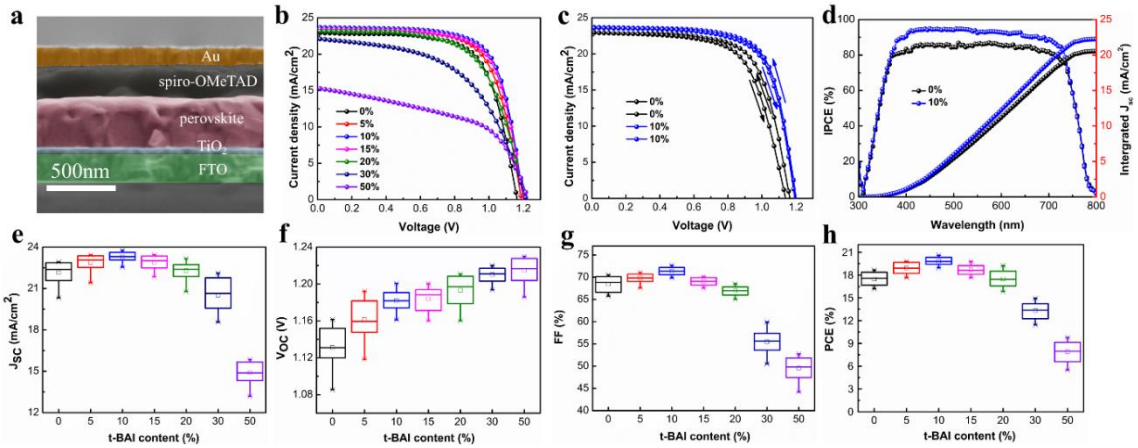

Fig. 2. Photovoltaic performances of t-$BA_x[Cs_{0.05}(FA_{0.83}MA_{0.17})_{0.95}]_{1-x}Pb(I_{0.83}Br_{0.17})_3$ perovskite solar cells. (a) cross sectional SEM images of perovskite solar cell (X = 10%) with complete device configuration of FTO/TiO_2/perovskite/spiro-OMeTAD/Au. (b) J–V curves of champion devices based on different t-BA percentages. (c) J–V curves of the devices employing X = 0% and X = 10% from forward bias to short circuit (FB-SC) and from short circuit to forward bias (SC-FB) scans. (d) IPCE spectra and integrated current density of champion devices based on X = 0% and X = 10% perovskites. (e-h) Statistical data for J_{SC}, V_{OC}, FF and PCE obtained from 20 cells per condition prepared with different t-BA percentages.

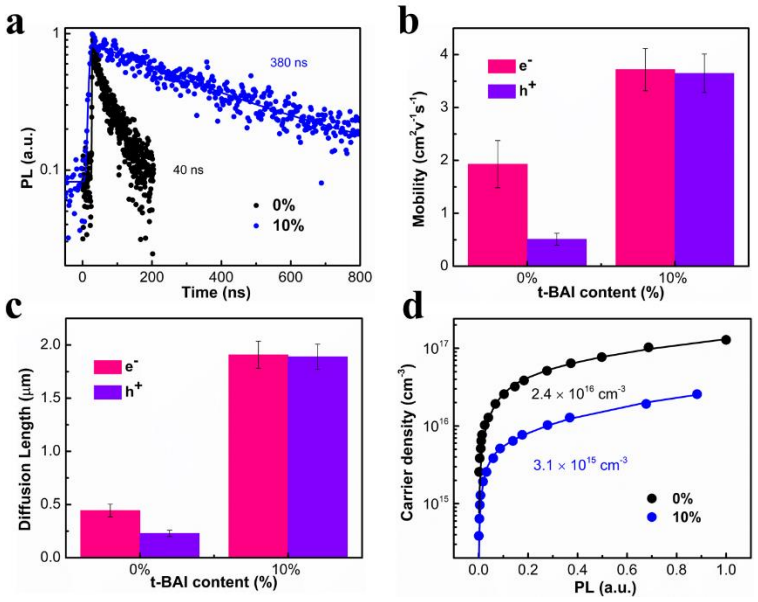

Fig. 3. Optoelectronic properties of $Cs_{0.05}(FA_{0.83}MA_{0.17})_{0.95}Pb(I_{0.83}Br_{0.17})_3$ and t-$BA_{0.1}[Cs_{0.05}(FA_{0.83}MA_{0.17})_{0.95}]_{0.9}Pb(I_{0.83}Br_{0.17})_3$ perovskite films. (a) Time-resolved photoluminescence (TRPL) decay curves of perovskite films with X = 0% and X = 10%. (b) Charge carrier mobilities in X = 0% and X = 10% perovskite films. (c) Charge carrier diffusion lengths in X = 0% and X = 10% perovskite films. (d) PL intensity as a function of photon-generated exciton density within the low pump fluence range in X = 0% and X = 10% perovskite films.

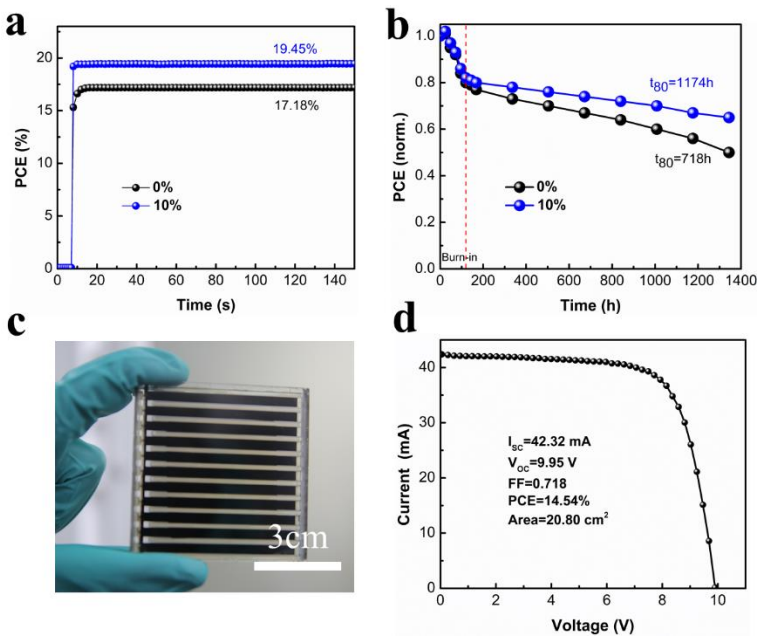

Fig. 4. Stability and large-area solar cells. (a) maximum power point (MPP) tracking under 1 Sun AM1.5G illumination measured in air, for X = 0% and X = 10% devices. (b) Stability test of perovskite solar cells (X = 0% and 10%) under continuous light illumination (AM1.5G, 100 mW cm^{-2}) in an ambient environment at 45-50 ^{o}C and with 45-55% humidity. (c) Image of a 6×6 cm^2 module. (d) J–V curve using the X = 10% perovskite in a 6×6 cm^2 module.

Table 1. Photovoltaic parameter. The detailed photovoltaic parameter of PSCs devices based on t-$BA_x[Cs_{0.05}(FA_{0.83}MA_{0.17})_{0.95}]_{1-x}Pb(I_{0.83}Br_{0.17})_3$ with various X value. Average device characteristics with standard deviation were obtained on the basis of 20 cells for each set.

t-BA (%)	Devices	J_{SC} (mA/cm^2)	V_{OC} (V)	FF (%)	PCE (%)
0	Average	22.2±0.8	1.13±0.02	68.5±1.8	17.4±0.8
	Champion	22.93	1.16	70.21	18.67
5	Average	22.8±0.6	1.16±0.02	69.4±1.0	19.0±0.8
	Champion	23.43	1.19	71.05	19.81
10	Average	23.2±0.4	1.18±0.01	71.3±0.7	19.8±0.4
	Champion	23.68	1.20	72.57	20.62
15	Average	22.7±0.6	1.18±0.02	68.8±0.9	18.7±0.6
	Champion	23.45	1.20	70.34	19.79
20	Average	22.3±0.6	1.19±0.02	67.1±1.1	17.5±0.9
	Champion	23.18	1.21	68.58	19.23
30	Average	20.5±1.2	1.21±0.01	55.3±2.1	13.3±1.3
	Champion	22.12	1.22	55.37	14.94
50	Average	14.9±0.9	1.21±0.02	49.5±2.8	7.9±1.4
	Champion	15.37	1.23	51.75	9.78

Notes

The authors declare no competing financial interest.

Acknowledgements

The authors acknowledge the financial support from Macau Science and Technology Development Funds (FDCT-116/2016/A3, FDCT-091/2017/A2, FDCT-014/2017/AMJ), Research Grants (SRG2016-00087-FST, MYRG2018-00148-IAPME) from University of Macau, the Natural Science Foundation of China (91733302, 61605073, 2015CB932200, and 11790293), and the Young 1000 Talents Global Recruitment Program of China. T.C.S. acknowledges the financial support from the JSPS-NTU Joint Research Project M4082176; the Ministry of Education AcRF Tier 2 grants MOE2015-T2-2-015, MOE2016-T2-1-034, MOE2017-T2-1-110 and MOE2017-T2-2-002; and from the Singapore National Research Foundation through the NRF Investigator ship Programme NRF-NRFI-2018-04.

References

[1] A. Marchioro, J. Teuscher, D. Friedrich, M. Kunst, R. Van De Krol, T. Moehl, M. Grätzel, J.-E. Moser, Nature photon. 8 (2014) 250-255.

[2] K.-G. Lim, H.-B. Kim, J. Jeong, H. Kim, J. Y. Kim, T.-W. Lee, Adv. Mater. 26 (2014) 6461-6466.

[3] C. Wehrenfennig, M. Liu, H. J. Snaith, M. B. Johnston, L. M. Herz, Energy Environ. Sci. 7 (2014) 2269-2275.

[4] V. D'Innocenzo, G. Grancini, M. J. Alcocer, A. R. S. Kandada, S. D. Stranks, M. M. Lee, G. Lanzani, H. J. Snaith, A. Petrozza, Nat. Commun. 5 (2014) 3586.

[5] K. Wang, S. Wang, S. Xiao, Q. Song, Adv. Optical Mater. 6 (2018) 1800278.

[6] G. Xing, N. Mathews, S. Sun, S. S. Lim, Y. M. Lam, M. Grätzel, S. Mhaisalkar, T. C. Sum, Science 342 (2013) 344-347.

[7] Y. Yang, M. Yang, D. T. Moore, Y. Yan, E. M. Miller, K. Zhu, M. C. Beard, Nat. Energy 2 (2017) 16207.

[8] W. S. Yang, B.-W. Park, E. H. Jung, N. J. Jeon, Y. C. Kim, D. U. Lee, S. S. Shin, J. Seo, E. K. Kim, J. H. Noh, Science 356 (2017) 1376-1379.

[9] Y. Chen, T. Chen, L. Dai, Adv. Mater. 27 (2015) 1053-1059.

[10] F. Hao, C. C. Stoumpos, D. H. Cao, R. P. Chang, M. G. Kanatzidis, Nature Photon. 8 (2014) 489-494.

[11] H. J. Snaith, J. Phys. Chem. Lett. 4 (2013) 3623-3630.

[12] H. Kim, K.-G. Lim, T.-W. Lee, Energy Environ. Sci. 9 (2016) 12-30.

[13] J. A. Christians, P. A. Miranda Herrera, P. V. Kamat, J. Am. Chem. Soc. 137 (2015) 1530-1538.

[14] W. S. Yang, J. H. Noh, N. J. Jeon, Y. C. Kim, S. Ryu, J. Seo, S. I. Seok, Science 348 (2015) 1234-1237.

[15] N. J. Jeon, J. H. Noh, W. S. Yang, Y. C. Kim, S. Ryu, J. Seo, S. I. Seok, Nature, 517 (2015) 476.

[16] D. P. McMeekin, G. Sadoughi, W. Rehman, G. E. Eperon, M. Saliba, M. T. Hörantner, A. Haghighirad, N. Sakai, L. Korte, B. Rech, Science 351 (2016) 151-155.

[17] M. Saliba, T. Matsui, J.-Y. Seo, K. Domanski, J.-P. Correa-Baena, M.K. Nazeeruddin, S.M. Zakeeruddin, W. Tress, A. Abate, A. Hagfeldt, Energy Environ. Sci 9 (2016) 1989-1997.

[18] I. C. Smith, E. T. Hoke, D. Solis-Ibarra, M. D. McGehee, H. I. Karunadasa, Angew. Chem. Int. Ed. 126 (2014) 11414-11417.

[19] D. H. Cao, C. C. Stoumpos, O. K. Farha, J. T. Hupp, M. G. Kanatzidis, J. Am. Chem. Soc. 137 (2015) 7843-7850.

[20] H. Tsai, W. Nie, J.-C. Blancon, C. C. Stoumpos, R. Asadpour, B. Harutyunyan, A. J. Neukirch, R. Verduzco, J. J. Crochet, S. Tretiak, Nature 536 (2016) 312.

[21] X. Zhang, X. Ren, B. Liu, R. Munir, X. Zhu, D. Yang, J. Li, Y. Liu, D.-M. Smilgies, R. Li, Energy Environ. Sci. 10 (2017) 2095-2102.

[22] R. L. Milot, R. J. Sutton, G. E. Eperon, A. A. Haghighirad, J. Martinez Hardigree, L. Miranda, H. J. Snaith, M. B. Johnston, L. M. Herz, Nano Lett. 16 (2016) 7001-7007.

[23] L. N. Quan, M. Yuan, R. Comin, O. Voznyy, E. M. Beauregard, S. Hoogland, A. Buin, A. R. Kirmani, K. Zhao, A. Amassian, J. Am. Chem. Soc. 138 (2016) 2649-2655.

[24] K. Yao, X. Wang, Y.-X. Xu, F. Li, L. Zhou, Chem. Mater. 28 (2016) 3131-3138.

[25] G. Xing, B. Wu, X. Wu, M. Li, B. Du, Q. Wei, J. Guo, E. K. Yeow, T. C. Sum, W. Huang, Nature Commun. 8 (2017) 14558.

[26] A. D. Jodlowski, C. Roldán-Carmona, G. Grancini, M. Salado, M. Ralaiarisoa, S. Ahmad, N. Koch, L. Camacho, G. De Miguel, M. K. Nazeeruddin, Nat. Energy 2 (2017) 972-979.

[27] N. Rolston, A. D. Printz, J. M. Tracy, H. C. Weerasinghe, D. Vak, L. J. Haur, A. Priyadarshi, N. Mathews, D. J. Slotcavage, M. D. McGehee, Adv. Energy Mater. 8 (2018) 1702116.

[28] T. Bu, X. Liu, Y. Zhou, J. Yi, X. Huang, L. Luo, J. Xiao, Z. Ku, Y. Peng, F. Huang, Energy Environ. Sci. 10 (2017) 2509-2515.

[29] V. Milman, B. Winkler, J. White, C. Pickard, M. Payne, E. Akhmatskaya, R. Nobes, Int. J. Quant. Chem. 77 (2000) 895-910.

[30] M. Segall, P. J. Lindan, M. A. Probert, C. J. Pickard, P. J. Hasnip, S. Clark, M. Payne, J. Phys.: Condens. Matter 14 (2002) 2717.

[31] Y.-Y. Zhang, S. Chen, P. Xu, H. Xiang, X.-G. Gong, A. Walsh, S.-H. Wei, Chin. Phys. Lett. 35 (2018) 036104.

[32] G. Nagabhushana, R. Shivaramaiah, A. Navrotsky, Proc. Nati. Acad. Sci. 113 (2016) 7717-7721.

[33] X. Zeng, T. Zhou, C. Leng, Z. Zang, M. Wang, W. Hu, X. Tang, S. Lu, L. Fang, M. Zhou, J. Mater. Chem. A 5 (2017) 17499-17505.

[34] D. Luo, W. Yang, Z. Wang, A. Sadhanala, Q. Hu, R. Su, R. Shivanna, G. F. Trindade, J. F. Watts, Z. Xu, Science 360 (2018) 1442-1446.

[35] C. Liang, P. Li, H. Gu, Y. Zhang, F. Li, Y. Song, G. Shao, N. Mathews, G. Xing, Sol. RRL 2 (2018) 1700217.

[36] J. H. Heo, D. H. Song, H. J. Han, S. Y. Kim, J. H. Kim, D. Kim, H. W. Shin, T. K. Ahn, C. Wolf, T.-W. Lee, S. H. Im, Adv. Mater. 27 (2015) 3424-3430.

[37] S. D. Stranks, G. E. Eperon, G. Grancini, C. Menelaou, M. J. P. Alcocer, T. Leijtens, L. M. Herz, A. Petrozza, H. J. Snaith, Science 342 (2013) 341-344.

[38] R. Younts, H.-S. Duan, B. Gautam, B. Saparov. J. Liu, C. Mongin, F. N. Castellano, D. B. Mitzi, K. Gundogdu, Adv. Mater. 29 (2017) 1604278.

[39] G. Xing, N. Mathews, S. S. Lim, N. Yantara, X. Liu, D. Sabba, M. Grätzel, S. Mhaisalkar, T. C. Sum, Nat. Mater. 13 (2014) 476-480.

[40] B. Jeong, S. M. Cho, S. H. Cho, J. H. Lee, I. Hwang, S. K. Hwang, J. Cho, T.-W. Lee, C. Park, Phys. Status Solidi Rapid Res. Lett. 10 (2016) 381-387.

[41] Z. Wang, Q. Lin, F. P. Chmiel, N. Sakai, L. M. Herz, H. J. Snaith, Nat. Energy 2 (2017) 17135.

[42] J. M. Azpiroz, E. Mosconi, J. Bisquert, F. De Angelis, Energy Environ. Sci. 8 (2015) 2118-2127.

Chao Liang graduated with a B.S. from Henan University of Technology (2014) as well as a M.S. in Materials Science from Zhengzhou University (2017). He is currently a Ph.D. candidate in the Institute of Applied Physics and Materials Engineering at University of Macau under the supervision of Professor Guichuan Xing. His research areas focus on perovskite solar cells and quantum dot solar cells.

Dandan Zhao graduated from Henan University in 2016 with master's degree, focusing on the solution-processed CIGS thin film solar cells. And she is currently a Ph.D. candidate in the Institute of Applied Physics and Materials Engineering at University of Macau under the supervision of Professor Guichuan Xing, and interest in using the new perovskite-like materials to fabricate stable solar cells.

Pengwei Li received his master's degree from ZhengZhou University in 2017. Now, he is currently working toward the Ph.D. degree under the Prof. Yanlin Song at Institute of Chemistry, Chinese Academy of Sciences (ICCAS). His research interest is printing photoelectric devices such as solar cells, thin film transistors, photo detectors and light-emitting diodes.

Bo Wu obtained his Ph.D. degree in physics from Nanyang Technological University (2014) and B.S. degree in physics from Beijing Normal University (2009). Currently he is a professor in the Institute of Electronic Paper Displays, South China Academy of Advanced Optoelectronics, South China Normal University. His research interests include the photophysics of halide perovskites, organic solar cells and light-emitting devices.

Gu Hao obtained his M.S. in 2018 from Zhengzhou University. He received a B.S. in Material Science and Engineering from Henan University of Technology in 2015. He is engaged in research assistant study at Institute of Advanced Materials (IAM), Nanjing Tech University, Nanjing, China. Most recently, his focus has been on a family of perovskite-based organic–inorganic hybrids, with the goal of creating useful materials for solar cell and light-emitting device applications.

Jiacheng Zhang received his B.S. from Xi'an Jiaotong University in 2013. He is currently a Ph.D. candidate in State Key Laboratory for Strength and Vibration of Mechanical Structures at Xi'an Jiaotong University. His research interest focuses on the multiscale modeling and materials design.

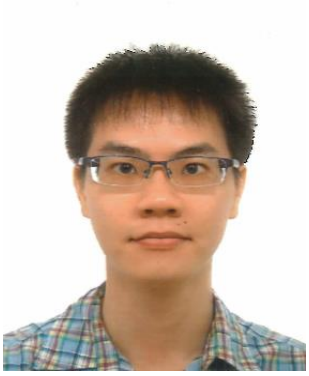

Teck Wee Goh obtained his B.Sc. degree in physics from Nanyang Technological University (2013). He is currently a final-year PhD candidate in the division of Physics and Applied Physics, School of Physical and Mathematical Sciences, Nanyang Technological University. His research interests include studying the surfaces and interfaces of halide perovskites using photoelectron spectroscopy.

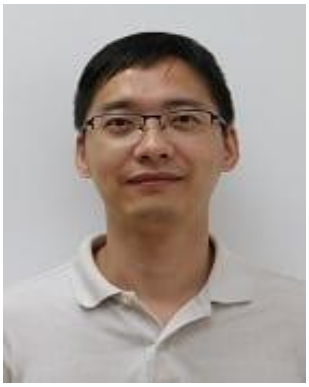

Shi Chen is an Assistant Professor in Institute of Applied Physics and Materials Engineering, University of Macau. He received Ph.D. degree in 2012 from National University of Singapore. His research interests are surface and interface physics, perovskite solar cell and 2D materials.

Yonghua Chen received a bachelor degree in Chemistry from Inner Mongolia University in 2006 and a Ph. D. in Polymer Chemistry and Physics at the Changchun Institute of Applied Chemistry, Chinese Academy of Sciences, in 2011. Afterward, he spent time at Wake Forest University (2 years) and Case Western Reserve University (2 years) as a postdoctoral researcher. He is currently a full professor at Nanjing Tech University. His research interests are organic and organic/inorganic hybrid optoelectronic materials and devices for flat panel displays and solid state lighting, and for energy conversion.

Zhendong Sha received his Ph.D. degree in Physics from National University of Singapore in 2011. He served on Institute of High Performance Computing as research scientist between 2010 and 2013. He joined Xi'an Jiaotong University as an Associate Professor in 2013 and became full Professor in 2018. His research interest is modeling and simulation of advanced structural and functional materials.

Guosheng Shao is currently the Director of State Centre for International Cooperation on Designer Low-carbon and Environmental Materials, Zhengzhou University and Founding Director of Zhengzhou Materials Genome Institute. He earned his PhD in Materials Science at University of Surrey in 1995 and thereupon worked as a senior research fellow, until transferring to Brunel University as Reader in Materials in 2005. He joined University of Bolton as Professor of Materials Modelling and Simulation in 2007. His academic interest is “designer” materials and application devices, focusing on sustainable energy systems and environmental technologies.

Tze Chien Sum received his BSc, MSc and Ph.D. in Physics from National University of Singapore in 1999, 2000, and 2005. He became an associate professor at Nanyang Technological University in 2014. His current research interests include Ultrafast optical spectroscopy and Time-integrated optical spectroscopy of emergent nanoscale and light harvesting material systems.

Guichuan Xing obtained his B. Sc. in 2003 at Fudan University and Ph.D. in 2011 at National University of Singapore. He joined IAM of Nanjing Tech University as a professor in 2014. His current research interest is nonlinear optical properties and ultrafast carrier dynamics in novel optoelectronic materials and devices.